

FY19 Los Alamos National Laboratory Experimental Campaigns at the Omega Laser Facility

P. A. Keiter, S. Palaniyappan, B. Scheiner, A. Rasmus, H. Johns, K. Meaney, K. Flippo, and Y. Kim

Los Alamos National Laboratory

Rayleigh–Taylor Instability Growth Measurements of Engineered Perturbations in Cylindrical Implosions

Principal Investigators: S. Palaniyappan, J. P. Sauppe, B. J. Tobias, C. F. Kawaguchi, K. A. Flippo, S. H. Batha, P. A. Bradley, E. N. Loomis, L. Kot, D. W. Schmidt, T. H. Day, R. Gonzales, and J. L. Kline (LANL); A. B. Zylstra and O. L. Landen (LLNL); D. Shvarts (Ben-Gurion University and NRCN); E. Malka (NRCN); and N. N. Vazirani (Virginia Tech)

Inertial confinement fusion (ICF) implosions require high convergence [convergence ratio (CR) of 17 for direct-drive implosions and CR of 30 to 35 for indirect-drive implosions] to achieve the required fuel density and temperature for ignition to occur. Radiation-hydrodynamic (rad-hydro) codes are an indispensable tool for designing current ICF experiments and a guide for future designs. Hydro-instability growth in ICF implosions is one of the major issues with the current ICF implosions that do not reach the predicted performances. The rad-hydro codes and the underlying physics models have not been validated against precise hydro-growth measurements at high convergence because such measurements simply do not exist. We have chosen cylindrical implosions to make precise hydro-growth measurements that can be used to validate the rad-hydro codes. We have performed cylindrical implosions with a CR of 2.5 at the University of Rochester’s Omega Laser Facility. We are planning to increase the CR using higher driver energy at Lawrence Livermore’s National Ignition Facility (NIF).

In FY19, we had two CylDRT shot days at the Omega Laser Facility. The first shot day was 14 March 2019, and the second shot day was 19 September 2019. The CylDRT platform was developed to measure the Rayleigh–Taylor (RT) growth of the engineered sine-wave initial perturbations on the inner side of an aluminum marker layer in cylindrical geometry. Both face-on and side-on x-radiographies were used as main diagnostics. Figure 1 shows the axial and transverse views of the nominal cylindrical target. The cylinder was 2.5 mm long and had a 986- μm outer diameter; the inner diameter of the cylinder was 860 μm . In the middle of the cylinder, there was a 500- μm -long aluminum marker band on the inner side of the cylinder. In addition, the inner aluminum layer had engineered sine-wave perturbations. Figure 2 shows the experimental geometry. The cylinder was driven by 40 beams with a 1-ns square pulse. A nickel backlighter was attached to the TIM-4 (ten-inch manipulator) end of the cylinder. An x-ray framing camera was used for face-on radiography in TIM-6. We used 12 \times magnification with a 10- μm pinhole onto a four-strip charge-coupled device [x-ray framing camera (XRFC3)]. We also used a TIM-2–TIM-3 side imaging of the target to see the uniformity of the implosion with a 6 \times magnification.

Figure 2 shows the experimental geometry from the VisRad. The cylinder is aligned along the P6–P7 axis. The TIM-4 backlighter is attached to the main cylinder target. The cylinder was inserted via TPS2 (Target Positioning System). The TIM-2–TIM-3 axis was used for the sidelighter imaging with a vanadium sidelight.

During the CylDRT19A shot day on 8 March, we measured the RT growth of single mode-20 initial sine-wave perturbations (Fig. 3). The measured growth rate of these engineered perturbations agrees well with the *xRAGE* hydro simulations. During the CylDRT19B shot day on 19 September, we measured the RT growth of surface roughness (200-nm and 500-nm) perturbations. This data have yet to be analyzed.

This material is based upon work supported by the Department of Energy National Nuclear Security Administration under Award Number DE-NA0003856, the University of Rochester, and the New York State Energy Research and Development Authority.

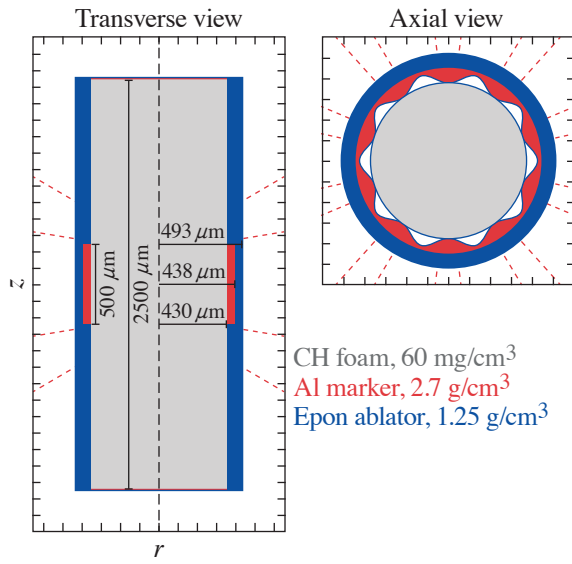


Figure 1
Sketch of transverse and axial views of the target.

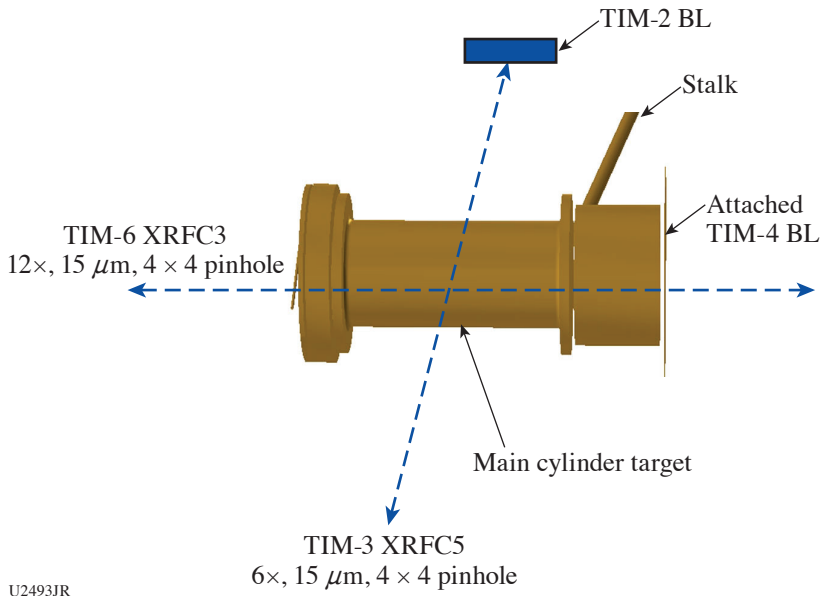


Figure 2
Experimental geometry for cylinder platform.
BL: backlighter.

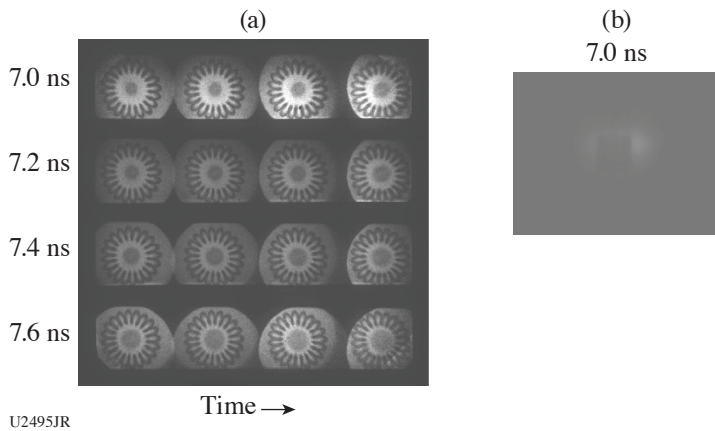


Figure 3
X-radiograph of the mode-20 sine-wave perturbation at a late time (7 to 7.8 ns). (a) Face-on view and (b) side-on view.

Evaluation of Revolver Shell Collisions

Principal Investigators: B. S. Scheiner (LANL and University of Iowa); M. J. Schmitt, S. C. Hsu, D. W. Schmidt, K. Molvig, N. Krasheninnikova, and C. Wilde (LANL); and F. J. Marshall, P. M. Nilson, D. N. Polsin, and T. R. Boehly (LLE); and J. G. Mance (Nevada National Security Site)

The Revolver-19A/B Campaigns evaluated the ablator-driver intershell collision relevant to the outer two shells of the *Revolver* triple shell direct-drive-ignition design.¹ Using scaled direct-drive double-shell, cone-in targets [Fig. 4(a)], these experiments aimed to validate the post-collision inner shell velocity predictions from the radiation-hydrodynamic code *HYDRA* using backlit images of the inner shell [Fig. 4(b)]. The measured inner shell velocity of 7.52 ± 0.59 cm/ μ s was in excellent agreement with the 7.19-cm/ μ s value predicted by *HYDRA* [Fig. 4(e)] without the need for any adjustable parameters in the simulation.² These experiments provide confidence in the modeling capability currently being used for the *Revolver* triple-shell ignition design, in particular, the ability to accurately model the shell collision process.

In addition to evaluating shell collisions, Revolver-19A/B developed a platform that is optimal for evaluating the feedthrough of RT unstable growth, seeded by drive asymmetries and engineering features, to the inner shell. High-resolution (~ 2.5 - μ m) images of the outer interface of the inner shell were obtained in Revolver-19B [Figs. 4(c) and 4(d)] through a collaboration between the LANL *Revolver* team and LLE. These images were the first obtained for a dynamic implosion using the newly commissioned Fresnel zone plate imager. Preliminary analysis of the sharp edge between the high-opacity inner shell and surrounding low-

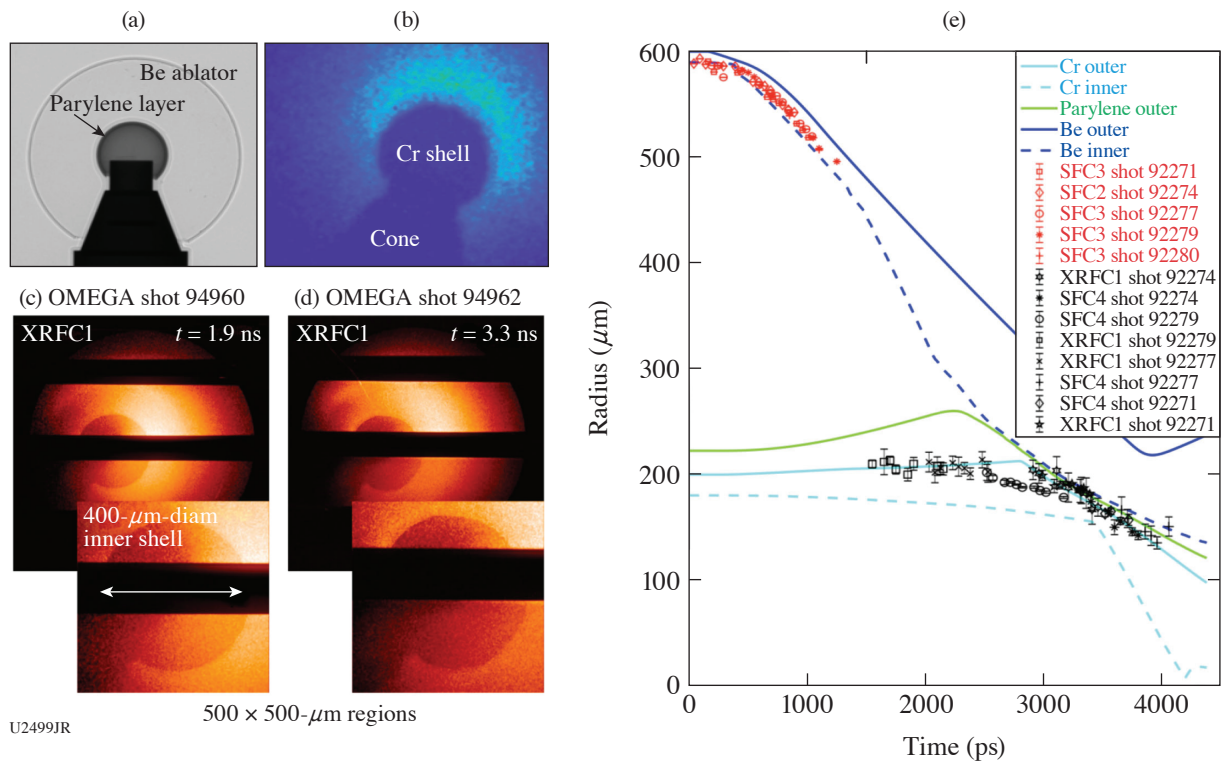


Figure 4

Summary of experimental and simulation data from Revolver-19A/B. (a) A pre-shot radiograph of the cone-in-shell target showing the target construction. (b) A backlit image of the inner shell after the collision with the outer shell corresponding to one of the black data points in (e). (c) A ~ 2.5 - μ m-resolution backlit Fresnel zone plate image of the inner shell from Revolver-19B at $t = 1.9$ ns before the shell collision. (d) Similar to (c) but after the shell collision. (e) The measured outer radius from ablator self-emission images and inner shell backlit images compared with simulation predictions.

opacity tamping layer suggests that Legendre modes in excess of $\ell = 50$ can be obtained from such images. Previously, such high-mode studies would have only been possible using much larger capsules at the NIF. These advances will allow the timely evaluation of mitigation schemes for high-mode growth in multishell targets due to drive asymmetries and engineering features using subscale targets on the OMEGA Laser.

This research was supported by the Laboratory Directed Research and Development Program of Los Alamos National Laboratory under project number 20180051DR.

Discrete Vortex Model and ModCons

Principal Investigators: A. Rasmus, C. Di Stefano, K. Flippo, E. Merritt, F. Doss, A. Strickland, and D. Schmidt (LANL)

In FY19, the discrete vortex model (DVM) and ModCons EP were built on diagnostic development successes from FY18, increasing our ability to resolve instability evolution. DVM and ModCons utilize a shared experimental platform to study different aspects of hydrodynamic-instability growth on interfaces (see Fig. 5). Three long-pulse beams are used to create a semi-sustained shock, which drives instability growth. These campaigns utilize a Mn He $_{\alpha}$ (6.2-keV) backlighter, which is used in conjunction with a spherical crystal imager to create x-ray radiographs of interface evolution.

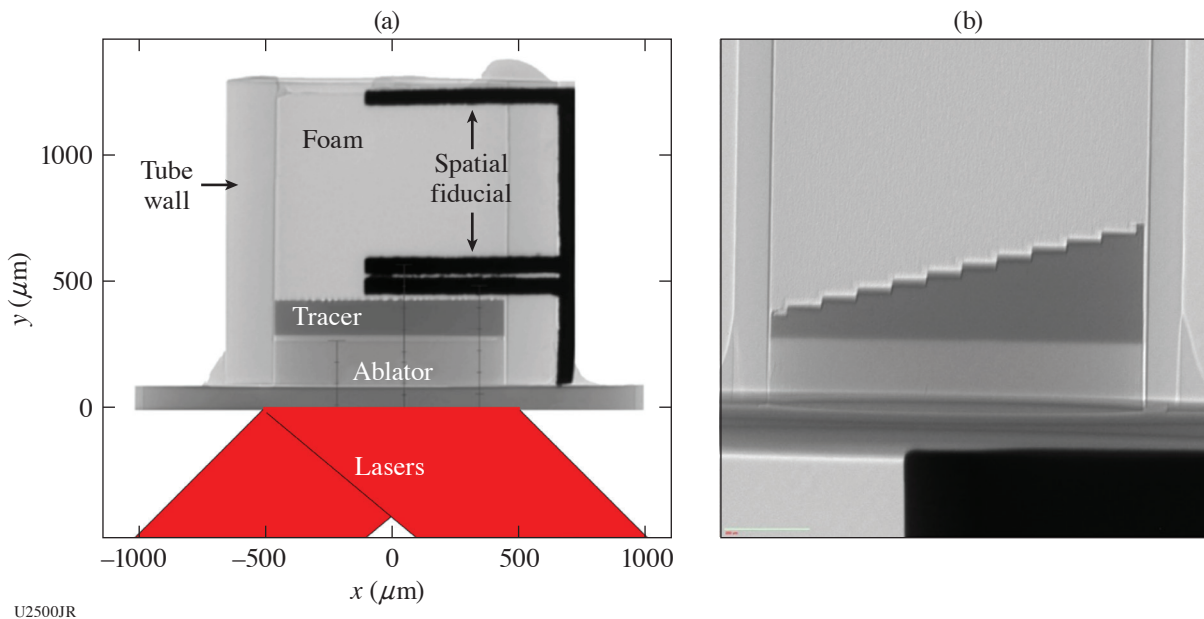


Figure 5

(a) A pre-shot radiograph of a ModCons target and (b) a pre-shot radiograph of a DVM target. Three lasers irradiate the ablator, driving a shock into the target. Hydrodynamic instability growth takes place at the interface between the tracer and foam.

ModCons-19A and ModCons-19B measured the evolution of Richtmyer–Meshkov (RM) growth, with delayed-onset Rayleigh–Taylor (RT), for a broadband perturbation [see Fig. 6(a)]. This yielded good measurements of coupled RM growth during the linear phase of instability evolution. These measurements will yield insight into how initially laminar multimode interfaces become nonlinear and eventually turbulent.

DVMEP-19A measured the evolution of a staircase perturbation [Fig. 6(b)]. This campaign is designed to show that whether the discrete vortex model describes the post-shock evolution of an interface depends on the vorticity distribution along the post-shock interface, rather than the type of vorticity. We also performed proof-of-concept shots for a target type that should allow us to measure the rate at which information about a vorticity distribution propagates through the post-shock system.

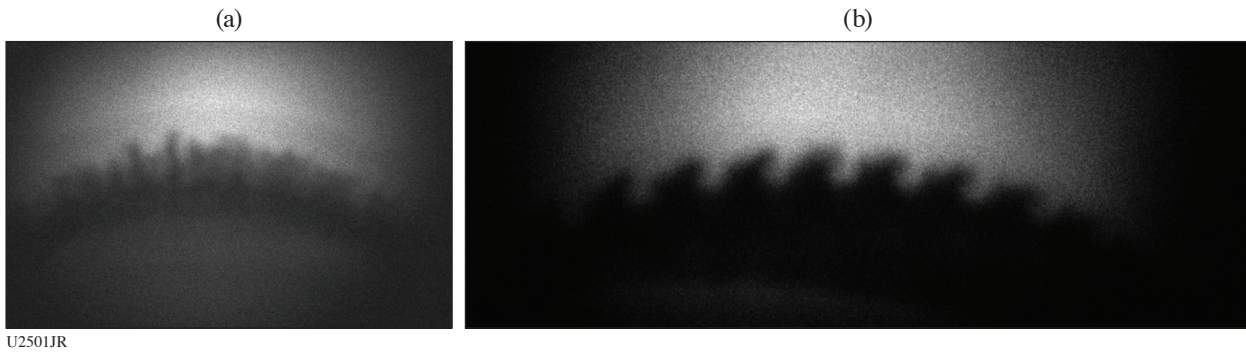


Figure 6
Experimental radiographs showing hydrodynamic instability growth: (a) ModCons and (b) DVM.

Radishock: The Evolution of Radiation Flow Across a Dynamic Boundary Provided by a Counter-Propagating Shock Using a Time Series of Shots of Space-Resolved Spectra and Radiography to Obtain Temperature and Density

Principal Investigators: H. M. Johns, P. Kozlowski, S. Wood, A. Liao, T. S. Perry, C. Fryer, C. J. Fontes, P. Hakel, J. P. Colgan, T. Urbatsch, and M. Douglas (LANL); and J. W. Morton and C. R. D. Brown (Atomic Weapons Establishment)

Radishock conducted three shot days on OMEGA this year: Radishock-19A, Radishock-19B, and Radishock-19C. The Radishock Campaign studies the interaction between a supersonic Marshak wave (generated by a hohlraum) and a counter-propagating shock (generated using a directly driven Be ablator). This system is a laboratory analogue to core-shell interactions in Type II_n, II_p, and superluminous supernovae. Additionally, this serves as a physics-based test of the COAX diagnostic platform. When the radiation flow meets the leading edge of the counter-propagating shock, we observe a temperature spike that is larger than the uncertainties we expect in the COAX Platform in simulations (see Fig. 7). As in COAX, we measure the temperature using absorption spectra generated when our Ti-laden aerogel foam is ionized by our radiation front to a temperature of 100 to 150 eV. When we backlight this plasma with 4.5- to 5.5-keV x rays generated by our Kr capsule backlighter, the L-shell Ti ions absorb those photons, resulting in $1s-2p$ and $1s-3p$ K-shell spectra that are very temperature sensitive due to their source in L-shell ions.

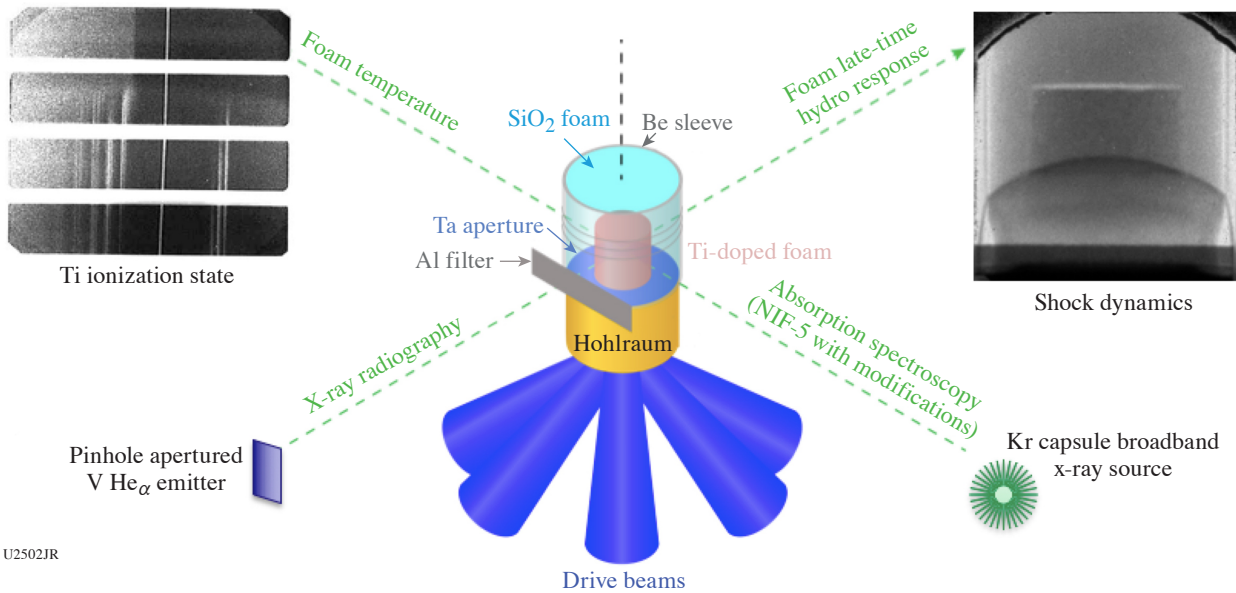
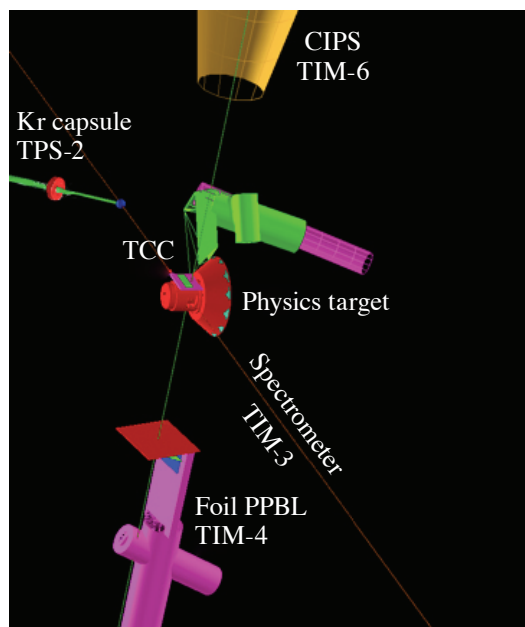


Figure 7
COAX Platform image showing quasi-perpendicular spectroscopic and hydrodynamic axes.

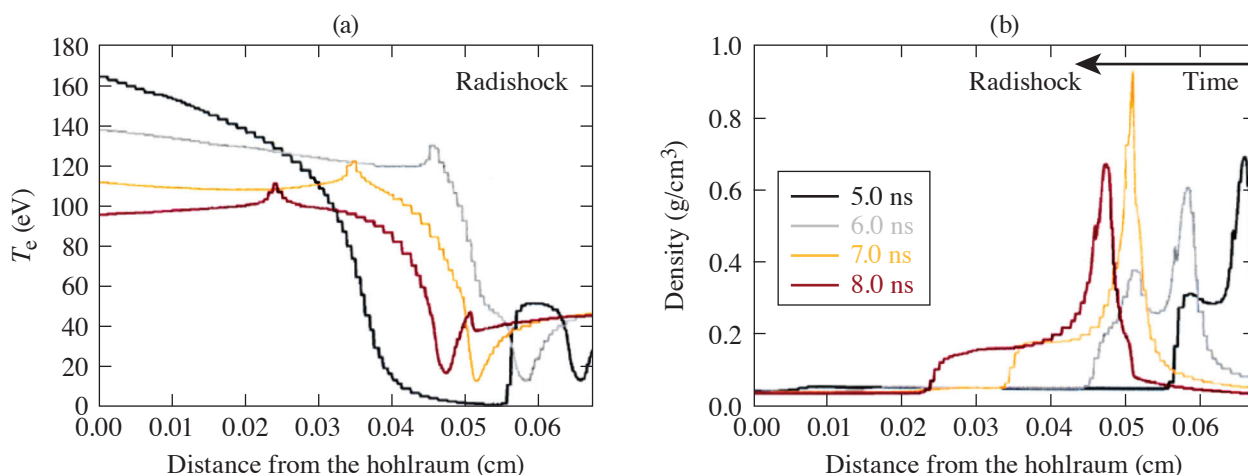
The other axis of our system enables us to view the hydrodynamic behavior and determine the location and eventual density of the shock. In this case we backlight the target with a V-foil backlighter attached to a substrate with a pinhole in it. In both cases we are using point-projection backlighting. Figure 8 shows the platform with the Radishock physics target.



U2503JR

Figure 8
Radishock platform in VisRad. PPBL: point-projection backlighter.

Time zero in Radishock is the start of the ablator drive. The hohlraum drive starts at 4 ns after the ablator drive, but instead of being a single 1-ns square pulse, the 12 beams are divided into two sets of six beams, where the second set is delayed by 1 ns (starting at 5 ns) with respect to the first set. While this reduces the temperature achieved, this longer drive helps the radiation flow to stay supersonic longer, which maximizes the amount of time we have to conduct our experiment. To record spectroscopic or radiography data at different times, we change the relative timing between when we fire the capsule or V-foil backlighter so that we can record spectra or radiographs at different times in the evolution of this system, but the relative hohlraum timing or ablator timing remain unchanged. Figure 9 shows simulations of Radishock at 5, 6, 7, and 8 ns after the ablator drive. These



U2504JR

Figure 9
Simulations of Radishock experiment (a) T_e and (b) density at different data collection times.

represent times at which we could collect data to observe pre-interaction (5 ns), start of interaction (6 ns), peak density (7 ns), and late-time interaction (8 ns). These simulations show temperature for the radiation front interacting with the shock on the left and density on the right.

In Fig. 10, the hohlraum is positioned at 0 cm on the left, and the clipper is on the right side. The distance between the two is about 650 μm .

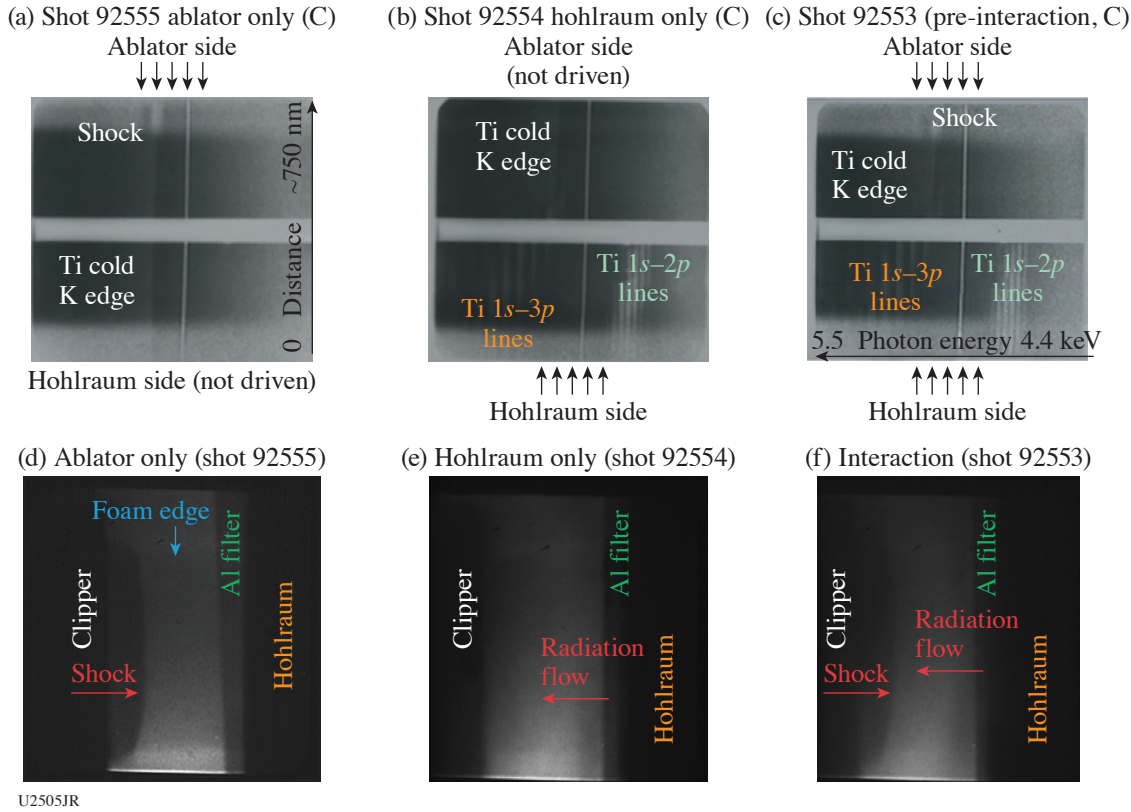


Figure 10 [(a)–(c)] Spectra, [(d)–(f)] radiography from Radishock-19A for the [(a),(d)] ablator only, [(b),(e)] radiation-flow only, and [(c),(f)] interaction. Radiography was taken at ~ 5.8 ns for these three shots.

Table I summarizes the types of data collected in Radishock-19A, 19B, and 19C, where 19B was a characterization day instead of a nominal characterization day. In Radishock-19A we focused on the start of interaction and peak density. In Radishock-19C we focused on peak density and late-time behavior. In FY18 we had a problem with our radiography involving an early-light effect, which we have determined was due mostly to a mix between soft x rays generated by the CH tube that contains the Radishock

Table I: Data type of shots collected and total number of shots/shot day in FY19.

Day	Date	Spectra	Radiography	DANTE and SOP	V-foil spectra	Number of shots
19A	1/31/19	5 ns, 6.2 ns	5.8 ns, 7.2 ns	–	–	14
19B	9/12/19	–	–	2 COAX and 7 Radishock hohlraums	4 shots	13
19C	8/15/19	7.2 ns, 8.2 ns	4.7 ns, 8.3 ns	–	–	12

SOP: streaked optical pyrometer

foam and blowoff from the Be ablator. In Radishock-19A we added a cone to block the x rays from the ablator blowoff from being recorded by the close-in ported snout (CIPS's) tip and added additional Be shielding on the target on the radiography side to block soft x rays from the CH tube from being recorded by the radiograph. Radishock-19A was the first time we fielded these platform changes, which successfully ameliorated the early light.

In Radishock-19B (12 September 2019) we instead collected data to characterize our hohlraums and our radiography back-lighter. We collected nine shots of hohlraum data for DANTE and streaked optical pyrometer (SOP) [with the OATEL (off-axis active shock breakout telescope) in the P1–P12 configuration]. DANTE was used to collect data from the hohlraum laser entrance hole, same as for our nominal configurations, but with the hohlraum near target chamber center (TCC) and no other sources (such as backlighters) in the chamber. We added a single-beam timing fiducial on a 2-mm V square, viewable by DANTE, to provide a small, short-duration signal that we could use to co-time the DANTE channels. The hohlraum included an Al foil on the radiation entrance holes that the hohlraum would heat, and we used the SOP to record the temperature of that plate to serve as a sanity check for simulations attempting to produce synthetic DANTE. Because nominal Radishock days have high incidence for DANTE and the hohlraum is not near TCC, and other radiation sources are present while the hohlraum is active, it becomes extremely challenging to analyze our DANTE data accurately. We intend to use the data from this 19B day to help us better understand what the hohlraum looks like alone, so that we can accurately separate out our hohlraum signal and backlighters on our nominal day. We also collected four shots of data on our V-foil backlighter spectrum to better identify which of the V $K_{\alpha,\beta}$ lines are actually providing the backlighting for our experiment and also confirmed that the emission did not last past the laser drive of our foil backlighter. We discovered that all three $K_{\alpha,\beta}$ are active, but the highest energy provides the strongest source. This will also be of help to better extract density from our radiographs. For these shots, we used the x-ray streak camera with the streaked x-ray spectrometer snout and XRS1 (Rowland x-ray spectrometer). We left DANTE on with no changes to identify any potential signal from the V-foil backlighters. There is a very small signal from this backlighter on several channels, but it is likely not detectable when the hohlraum is active. Figure 11 shows example lineouts from our SOP data for our Radishock hohlraums. Figure 12 shows examples of analyzed spectral data. The spectra shown are $1s-3p$ Ti K-shell spectra generated by L-shell ions. Each spectral feature is a blended set of transitions from a single ionization state. Higher photon energy features are from higher ionization stages; as such, more absorption in features at higher photon energy equates to a higher temperature. Whether the temperature difference is consistent with simulations shown in Fig. 9 at this time (6.2 ns) will require further analysis to determine. If the temperature spike is not present, however, we would expect the trend to be reversed—the radiation flow becomes cooler with distance from the hohlraum instead of hotter. Therefore, the deeper absorption observed at larger distances from the hohlraum is consistent with the existence of the temperature spike.

This work was performed under the auspices of the U.S. Department of Energy at Los Alamos National Laboratory under Contract No. 8923318CNA000001.

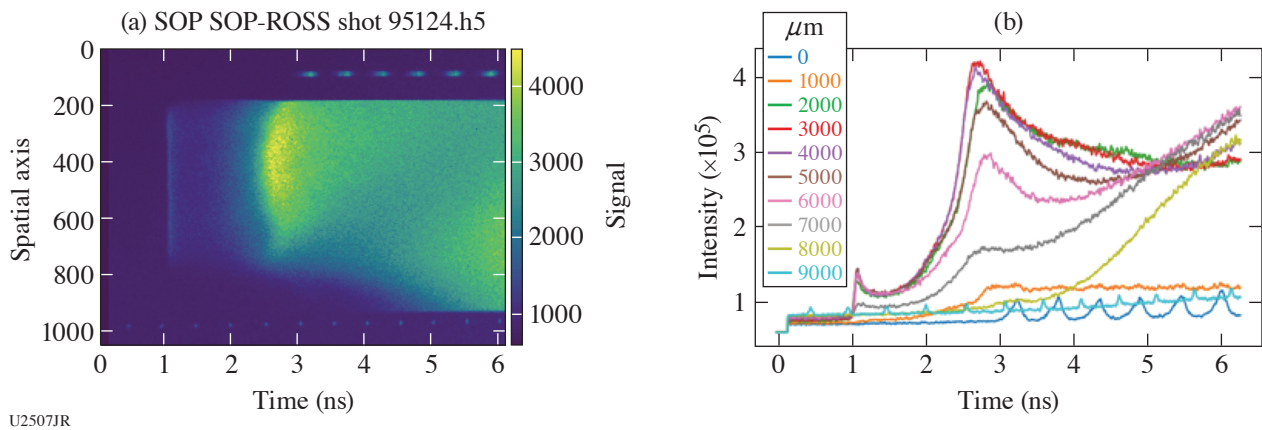


Figure 11
 (a) SOP data with (b) lineouts in time showing peak emission at just before 3 ns after the start of the hohlraum drive. ROSS: Rochester Optical Streak System.

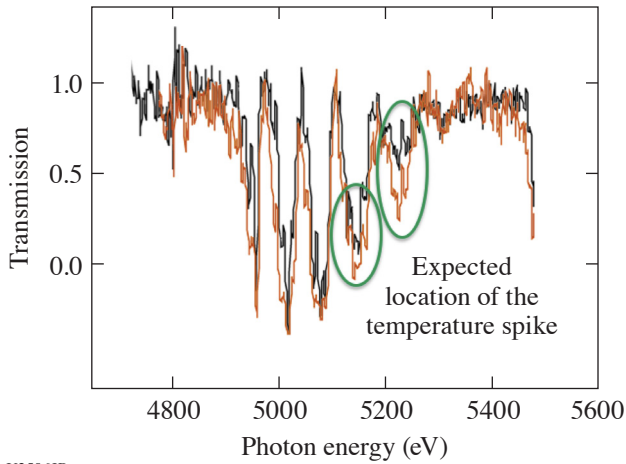


Figure 12
Transmission spectra from 19A interaction at 6.2 ns, at and behind the temperature spike.

U2506JR

High-Spatial-Resolution Separated Reaction Mix Measurements

Principal Investigators: K. D Meaney, Y. H. Kim, H. Herrmann, R. Gonzales, V. Garcia, and H. Geppert-Kleinrath (LANL); A. Leatherland (AWE); and A. Zylstra (LLNL)

Understanding the complex mixing processes that occur in ICF and high-energy-density systems is vital to improving performance. An OMEGA shot series in 2017 used a separated reactant platform to study mix but used very thin (150-nm) placed layers of deuterium fuel in 15- μm -thick CH plastic ablator shells around a hydrogen–tritium fuel in order to give a highly specific spatial location of shell mixture into the fuel. Previous separated reactant experiments had used 1- μm -thick or larger deuterium layers. The 2017 data revealed that 15- μm OMEGA capsules had two distinct mix measurements. When the layer was located right up against fuel, a high amount of mix was observed; when it was recessed just 0.3 μm and 0.6 μm away from the fuel, no mix of the shell was observed. This rapid dropoff of mix is believed to be caused by a diffusion-dominated mix state, which can occur when the yield is mostly shock dominated and hydrodynamic instabilities, such as Rayleigh–Taylor, do not have time to develop a turbulent mix layer. Interestingly, when the placed layer was recessed ever further to 0.9 μm , a significant amount of mix was again observed. This “inversion” mix suggests some mix mechanism that preferentially pulls material deeper away from the fuel.

Two OMEGA shot days in 2019 were executed to better understand the results from the 2017 shots. The shots in 2019 used a capsule design similar to that of 2017: spherical capsules with a placed deuterium layer (Fig. 13). First, to verify the hypothesis about the diffusion mix layer, a middle recession depth of 0.15 μm was placed between the high-mix layer (0- μm recession depth) and the no-mix layer (0.3 μm) to determine the diffusion length scale. The 2019 data show a sharp drop-off of mix, consistent with diffusion-dominated mix, but not as sharp as observed in 2017, possibly due to the capsules being 1 keV cooler than the

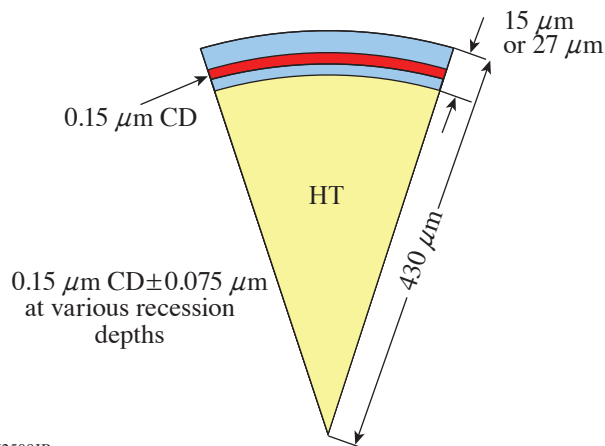


Figure 13
Diagram of the 2019 gamma-mix campaign capsules. All have <0.1% D fill.

U2508JR

2017 shots. Simulations of these cooler capsules to help understanding is ongoing. Second, by moving to thicker shells (27 μm) with different laser pulse shapes, the plasma conditions would be varied into a cooler but denser hot-spot condition (more NIF cryo DT-like), which are well understood to have a fully developed turbulent mix layer. By varying the plasma conditions, we should see a decrease in the steepness of the mixing layer as the capsules transition from diffusion dominated to hydrodynamically dominated. The 2019 data see a shallower mix drop-off as the capsules become cooler and denser. The summary of this data is shown in Fig. 14.

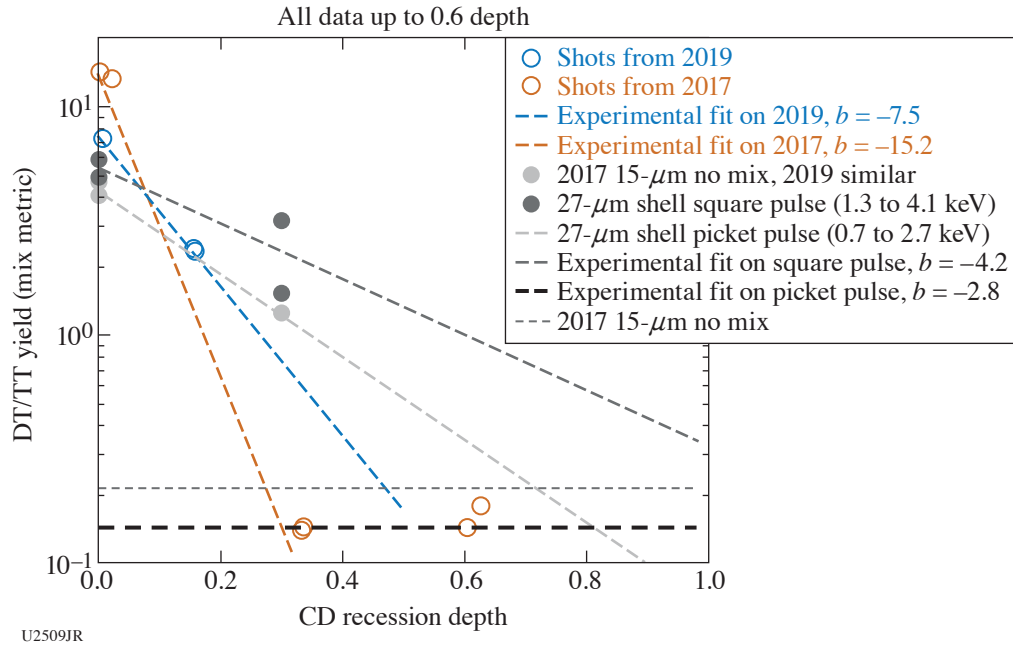


Figure 14
Comparison of how quickly the mix of the shell drops off at different temperature conditions.

The 2019 data also investigated the cause of the observed inversion mix seen at the 0.9- μm recession depth. Our initial hypothesis was that either a P1 asymmetry or a stalk-induced jet may cause preferential mixing further away from the fuel, pulling shell material from further out. This was tested by intentionally causing a larger P1 asymmetry by physically offsetting the capsules 50 and 100 μm from the target and laser center. The stalk was tested by placing multiple (two and four total) stalks called porcupine targets. Both of these variations observed no more increase in the mix at the 0.9- μm recession depth, suggesting neither has a substantial effect on the observed mix. Further recession depths were also tested at 1.4 μm and 2 μm and saw a further decreasing mix signal. All the data observed in both 2017 and 2019 are shown in Fig. 15.

The 2019 OMEGA data were successful in understanding complex mix mechanisms observed in 2017, but questions on the exact nature of the “mix dip” in the 0.3- and 0.6- μm recession depth and the relevance of diffusion dominated mix to NIF-like systems still remain and continue to be investigated.

The MShock Platform Studied Preheat Mitigation Strategies and Defect Evolution

Principal Investigators: K. A. Flippo, E. Merritt, T. Desjardins, F. Doss, C. Di Stefano, and A. Rasmus (LANL)

The MShock Campaign on OMEGA is a developmental test bed and design space for our premier hydrodynamic platform NIF MShock, a successor and derivative of the successful OMEGA and NIF Shock–Shear platform. The MShock Campaign vies to develop a versatile system for studying complex interfaces under the effects of successive shocks—either in co-propagating or counter-propagating geometries, or both combined. Here we can test ideas and develop techniques at a relatively low risk on a

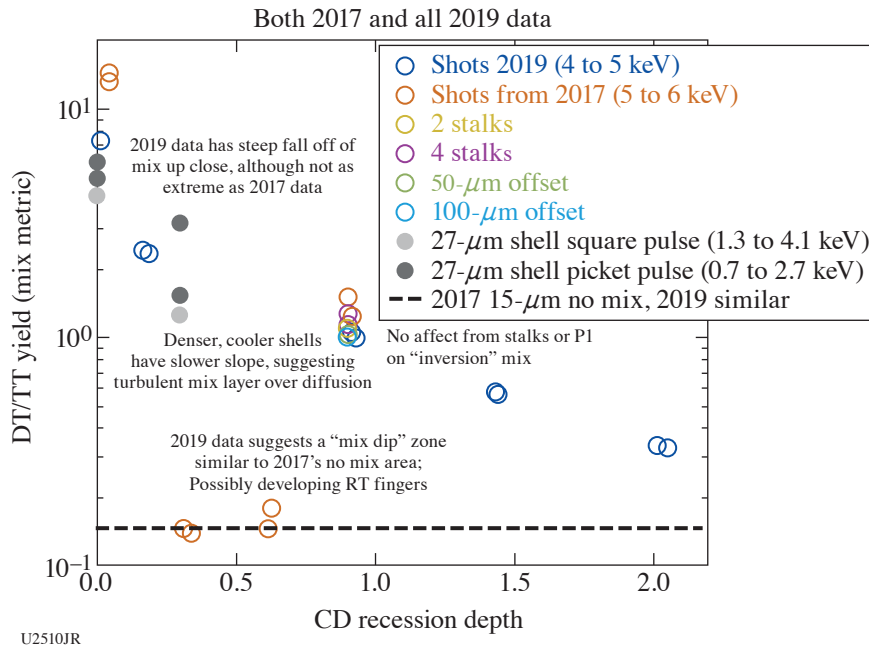


Figure 15
Summary of the mix data observed in 2019 with the data in 2017.

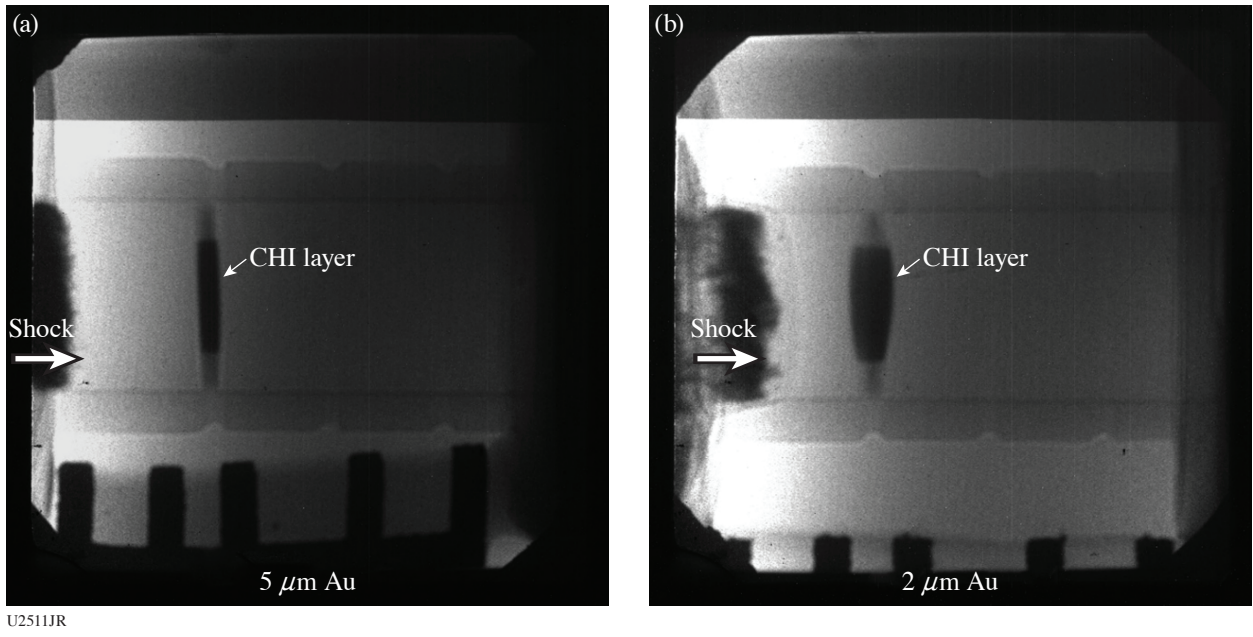
per-shot basis. This year we had three main goals: to test preheat mitigation strategies, develop a heating platform, and test jetting/defect concepts on the MShock platform.

We have tested several preheat mitigation strategies for the MShock platform with the secondary goal of minimizing the effects of those strategies on the shock strength, timing, and shape that drive the physics. We have tested a number of ablator types with various dopings and buried gold layers to damp hot electrons and x rays from the drive beams. This will be less necessary with the new phase plates that can accommodate our design needs; however, mitigation is still needed for higher drive strengths. The main ablator types tested were 1% to 3% iodine-doped CH, 1% to 3% Si-doped CH, and buried Au layers of 2 to 6 μm on the ablator surface inside the target or buried in the drive side. The iodine doping was shown to actually increase hot-electron production with the no-phase-plate drive configuration, so it was not useful. The thicker 5- μm Au layer slowed the shock down by about 3 ns compared to the no-Au layer but little preheat was observed (see Fig. 16). The thinner Au preheat layer did not slow the shock down significantly, but it also did not stop the preheat.

Another consequence of using the thicker 5- μm Au layer on the inside of the ablator was that at late time, the Au tended to obscure the physics [see Fig. 17(a)]. The layer was moved 65 μm inside the ablator to allow for more time before it would cloud the experiment, which worked well [Fig. 17(b)].

In conjunction, we have also been testing heating strategies to preheat our physics package at a time of our choosing, which requires us to have minimal preheat from the main drives. To this end, we have developed an MShock heater platform to study the effects of adding extra energy to the layer before and after initial shock or re-shock on OMEGA. The OMEGA version of the platform at this time is limited to shock and counter-propagating reshock. The layer expanded by a nearly a factor of 5 \times after heating and before first shock, indicating a temperature of several tens of eV.

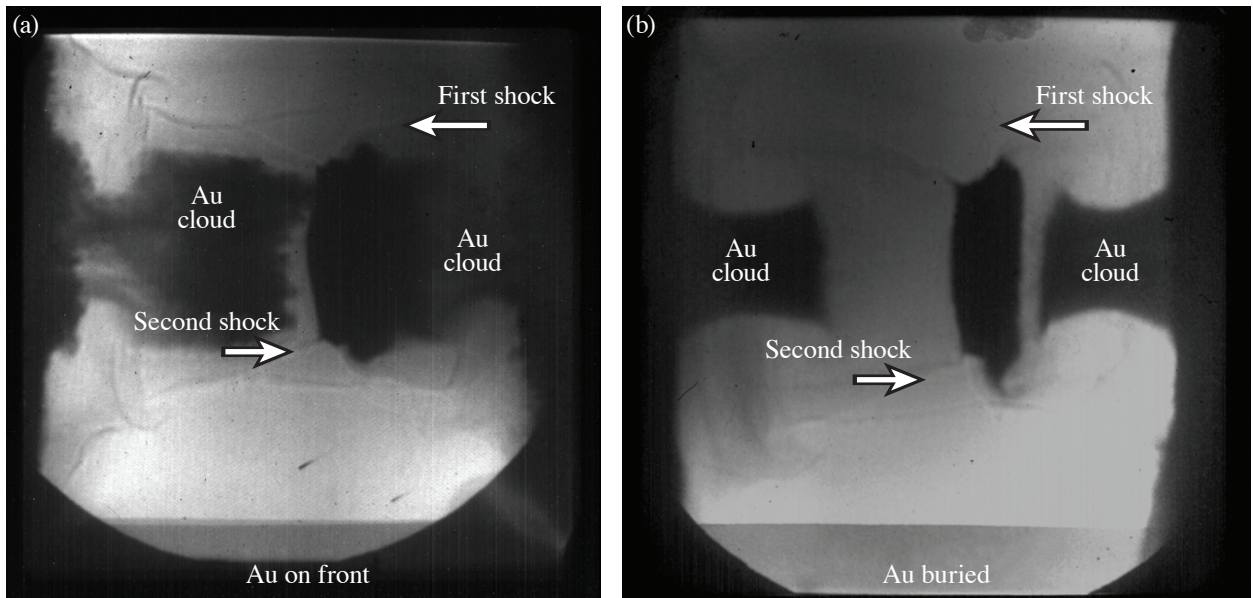
The third goal was to test the jet/defect platform. We used a doped central section with a divot to produce a jet from the shocked interface. The scaling of the layer thickness driven by a scaled problem led to the shock taking almost 10 ns to propagate across the PAI defect layer. This limited the growth of the jet in the geometry but did produce jetting from the divot and useful data to improve the platform (see Fig. 18).



U2511JR

Figure 16

(a) The 5- μm Au layer delays the shock by ~ 3 ns (4.5 ns after drive) with little preheat compared to (b) the 2- μm Au layer, which shows little delay but significant preheat. CHI: iodine-doped CH.



U2512JR

Figure 17

(a) The 5- μm Au design suffered from excessive Au clouding the physics. (b) When the Au was moved back into the ablator 65 μm , the Au was delayed sufficiently to allow one to see the physics of the interaction.

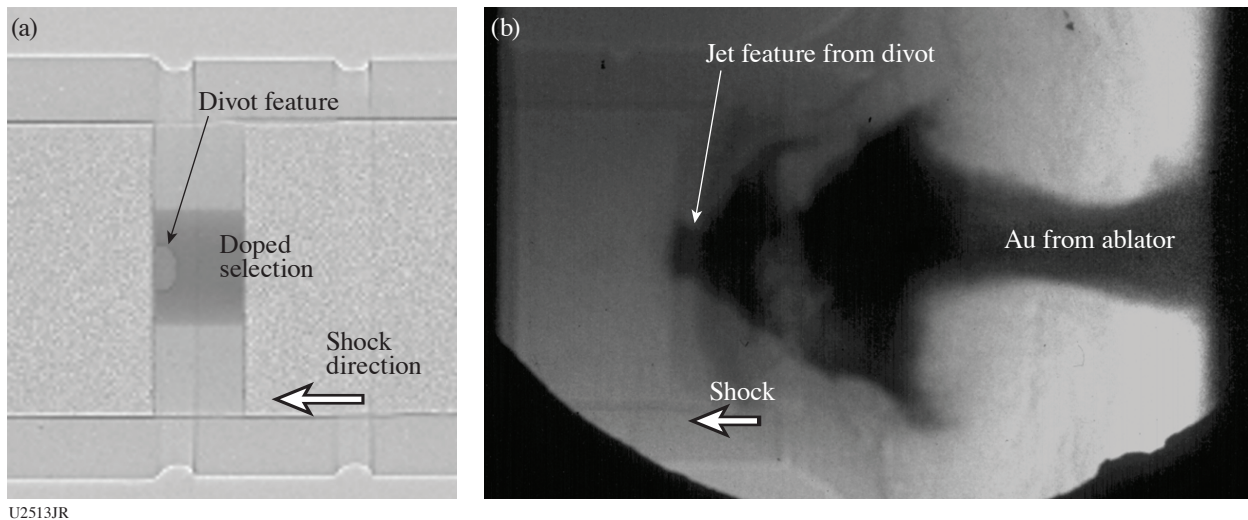


Figure 18
(a) Jet/divot target driven by (b) a strong shock.

The HEDB Campaign Explores If Magnetic Fields Change Turbulent Evolution of HED Systems

Principal Investigators: K. A. Flippo, Y. Lu, S. Li, D. H. Barnak,* H. Li, K. Kelso, A. Liao, A. Rasmus, N. Vazirani, and C. Fiedler Kawaguchi (LANL); E. Liang (Rice University); and C. K. Li, A. Birkel, and B. Lahmann (Massachusetts Institute of Technology)
*Currently at LLE

The HEDB Campaign is looking to quantify the scale and magnitude of self-generated B fields in high-energy-density (HED) systems and specifically to answer the question if these fields can change the turbulent evolution of these systems. This year's campaign focused on using D^3He implosions to produce protons for monoenergetic (14.7-MeV) proton radiography of HED-relevant platforms. We used a modified version of the Shock-Shear platform, where a set of two shocks counter-propagate across a layer, splitting the shock tube in half. This sets up a very strongly sheared layer with strong flows on either side for study. In these experiments we intentionally made a layer with slots in it so the shock can interact more strongly and lead to turbulence and B-field generation more quickly and of a large magnitude so that we would be sure to see them. We cut windows in the shock tube to allow the 14.7-MeV protons to traverse the internal structure, where the physics is occurring, without too much scattering; however, even with this help, the scattering is significant. To mitigate this effect, we employed a mask for the proton source, so that we would have an easier time differentiating scattering from B-field deflection. The mask is known as a "pepper pot." The HEDB experiment is shown in Fig. 19. In Fig. 19(a) the Be or CH shock tube is at the center with two gold cones on either side to prevent scattered light from the driver interaction from contaminating the x-ray imaging. The proton source is a D^3He capsule imploded 1 cm away from the main target, sending protons through the pepper-pot foil, through the "windows," and into the experiment. Proton radiography (pRad) images are shown in two columns: [(b) and (d)] show the synthetic pRad images using *FLASH* simulation results; [(c) and (e)] contain the experimental data. The top row [(b) and (c)] shows images with no fields present (turned off in *FLASH*) and an undriven target from the experiment. The bottom row [(d) and (e)] shows simulated fields of about 50 T from the *FLASH* results and the experimental results from a driven target. We estimate ~ 30 T from the measured deflection for the self-generated fields in the tube from these results. The next steps would be to improve the radiography by using a higher-flux short-pulse source from the OMEGA EP beamline into OMEGA on a joint shot day.

The LabDynamoEP Campaign Successfully Produced a Turbulent Magnetic Dynamo

Principal Investigators: K. A. Flippo, A. Liao, D. H. Barnak,* Y. Lu, S. Li, H. Li, A. Rasmus, K. Kelso, and C. Fiedler Kawaguchi (LANL); and C. C. Kuranz (University of Michigan)
*Currently at LLE

The LabDynamoEP Campaign is a turbulent magnetic dynamo (TMD) experiment using a simple cone design to produce a turbulent plume of plasma. For a TMD to form, the Reynolds number of the flow and the magnetic Reynolds number of the

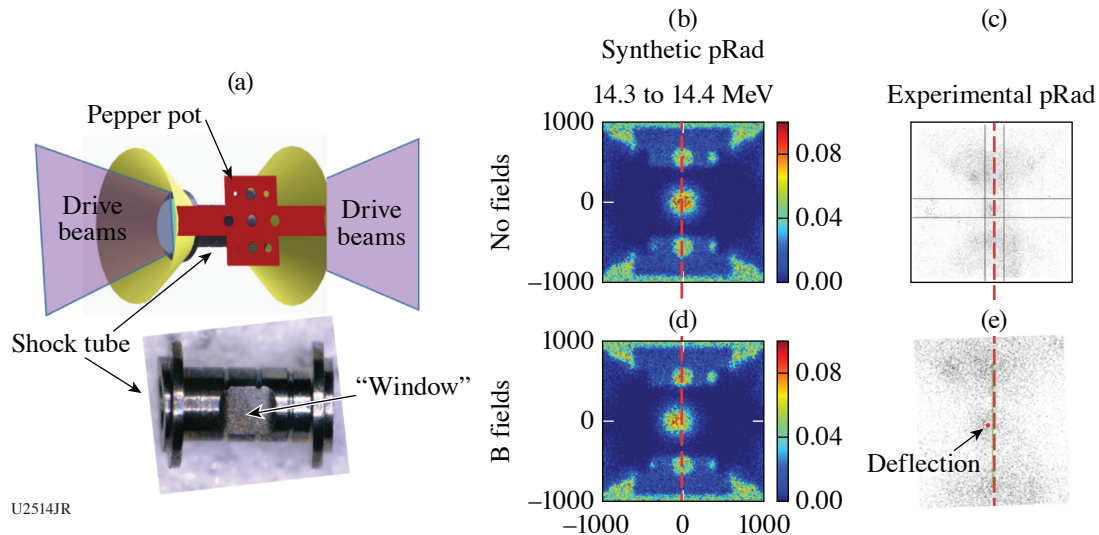


Figure 19

(a) HEDB setup; [(b)–(e)] Proton radiography (pRad). [(b),(c)] The pRad images have no fields (scattering only) and show no deflection off the center line (dashed red line); [(d),(e)] the pRad images have a 50-T field (synthetic) and an estimated 30-T field from experiment.

plasma must be both high and comparable. The ratio of these two numbers is known as the Prandtl number (Rm/Re), which can be rewritten as momentum diffusivity over thermal diffusivity or, alternatively, viscosity over thermal conductivity. When this ratio is of order unity or larger, then the TMD can operate. This platform is designed to achieve this goal on OMEGA EP (see Ref. 3).

We have obtained a series of proton radiographs using the fourth beam on OMEGA EP, which produced a target normal sheath accelerated (TNSA) proton beam. The proton radiographs can then be Fourier transformed into modal information to produce a power spectrum of the magnetic field modes (as in Fig. 20) following C. Graziani *et al.*⁴ Figure 21 shows the same for the experimental data from FY19 shots on OMEGA EP, with (a) proton radiographs and (b) reduced data. The solid colored curves represent different times in the *FLASH* simulation, and the dotted curves show the same for the experimental data. Both sets show the clear trend of growth of all modes, indicating the existence of a turbulent dynamo in action.

Preheat Effects on Macro-Pore MARBLE Foams

Principal Investigators: Y. Kim, P. Kozlowski, T. J. Murphy, T. H. Day, D. N. Woods, B. M. Haines, C. Di Stefano, and B. J. Albright (LANL)

In FY19, two Marble Void Collapse Campaigns on OMEGA were performed to provide supporting data for the Marble Implosion Campaign on the NIF. The NIF Marble capsules consist of deuterated foam whose pores are filled with tritium gas. Initial pore sizes are varied to adjust mix morphology. During the capsule implosion, however, hohlraum-driven x rays may increase the foam temperature, thereby reducing pore size and potentially wiping out macropore initial conditions. Diagnosing the pre-heat effects on the Marble foam on the NIF was not easily accessible; two OMEGA experiments were performed to assess and mitigate the effects of preheat on the Marble foam. The first approach was to develop an indirect-drive platform to identify the amount of x-ray preheat and the amount of shock-driven preheat. The second approach was to develop a direct-drive platform to measure the evolution of single-pore size, while varying the high-Z gas pressure in it.

Figure 22(a) shows the experimental setup utilizing a beryllium shock tube with an inner diameter of 500 μm . The ends of the tube are capped with Rexolite ablaters that can be doped with mid-Z materials such as up to 3% silicone. The ablator is irradiated by x-ray flux produced inside a gold hohlraum. To generate an x-ray drive, 20 beams of the 1-ns laser (total 10 kJ) are pointed at the inner wall of the gold hohlraum. The shock tube is filled with two pieces of low-density CH foams (40 mg/cm^3). A thin layer of plastic disk (40 μm thick) separates the two foam layers. The expansion of the thin layer hints at the amount of

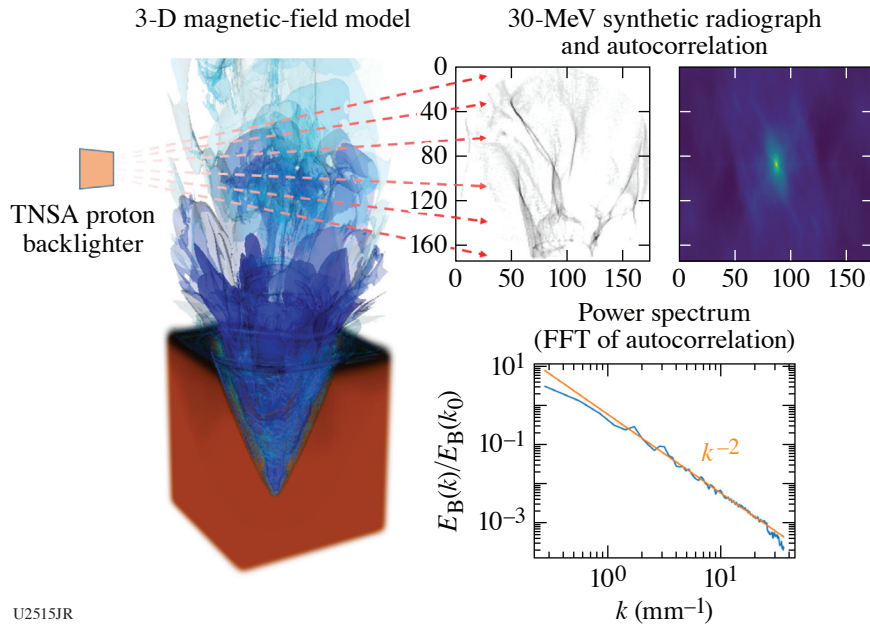


Figure 20

The LabDynamoEP setup is a simple cone of a few millimeters in size. Three OMEGA EP beams irradiate the cone nonuniformly to produce a turbulent plume of plasma. The lasers additionally heat the area above the cone, keeping the turbulent plasma hot and driving a turbulent magnetic dynamo. These data are a *FLASH* simulation with synthetically produced proton radiography (from the *FLASH* package) showing the k^{-2} spectrum one would expect from a turbulent compressible flow. FFT: fast Fourier transform.

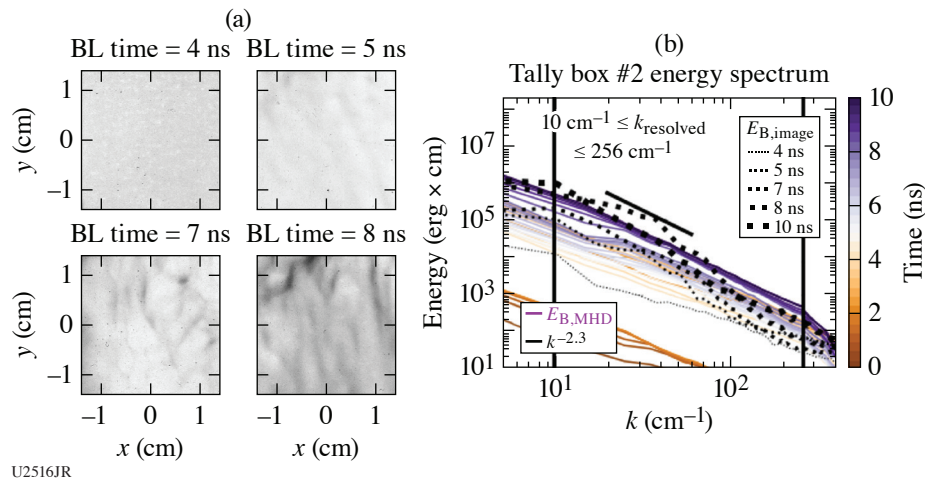


Figure 21

(a) Experimental proton radiographs of the TMD in action analyzed into (b) a power spectrum in time showing the growth of all modes in time (the solid colored curves are *FLASH* simulation results and the dotted curves are experiment data), indicating the dynamo in action magnifying the magnetic fields.

preheat deposited in the foam. Using a point-projection radiographic technique, expansion of the plastic disk has been observed. Figure 22(b) shows a net growth width ($L-L_0$) of the plastic disk as a function of time, where the initial thickness L_0 is $40 \mu\text{m}$ and the measured width is L . Within a diagnostic time period (0 to 8 ns), the expansion of the plastic disk showed two distinct behaviors: In early times (up to 4 ns), the expansion rate is approximately $3 \mu\text{m/ns}$ ($\sim 0.2\text{-eV}$ equivalent temperature). Between 4 and 8 ns, the expansion rate increased significantly ($\sim 10 \mu\text{m/ns}$ or 2-eV equivalent temperature). Currently, a LANL *xRAGE* simulation is underway to identify the amount of preheat from a hohlraum-driven x ray and a shock-driven radiation.

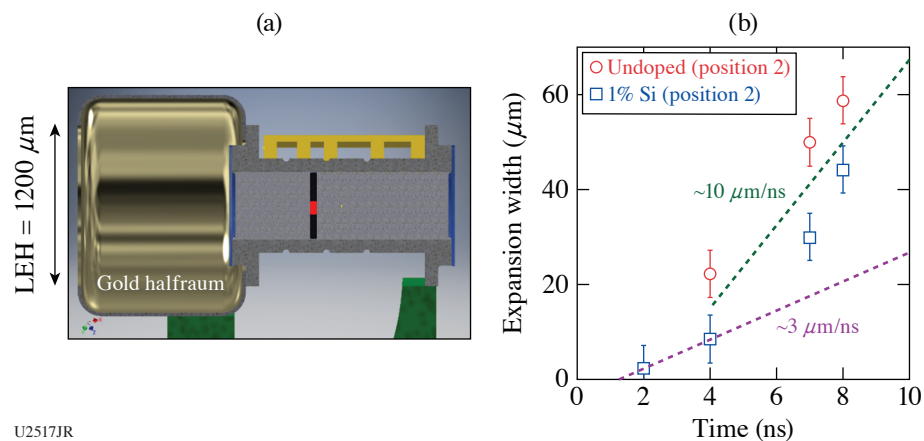
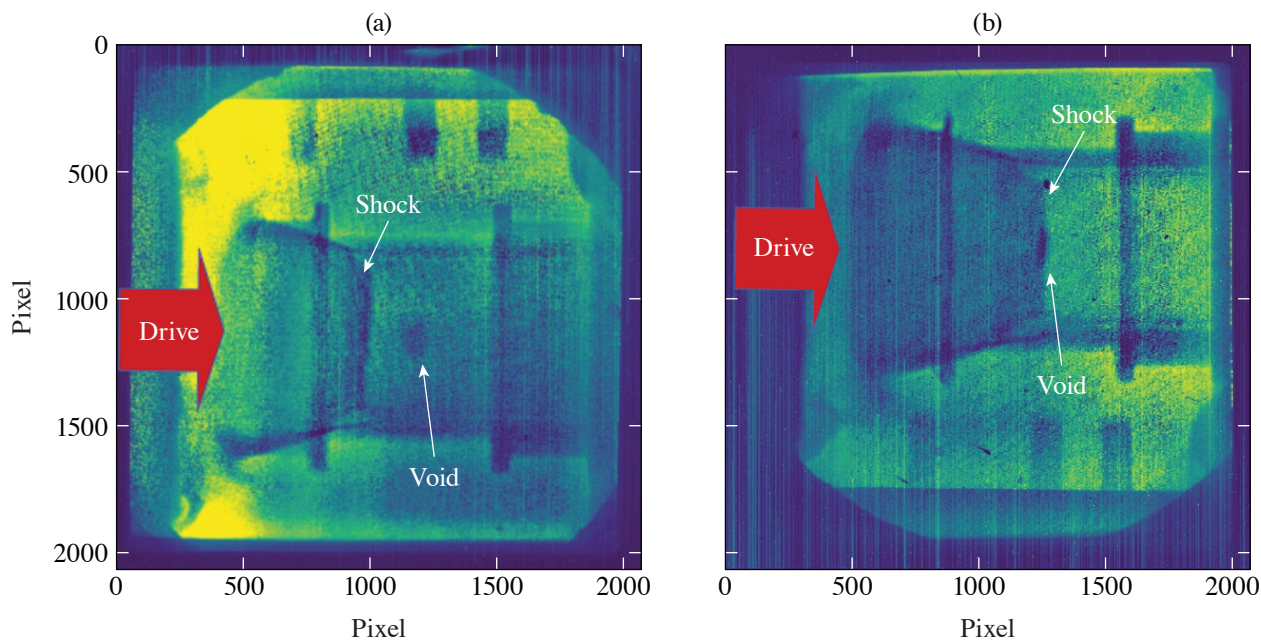


Figure 22

(a) Experimental schematics of indirect-drive preheat platform. (b) In early times (up to 4 ns), the expansion rate is approximately $3 \mu\text{m/ns}$ ($\sim 0.2 \text{ eV}$ equivalent temperature). Between 4 and 8 ns, the expansion rate increased significantly ($\sim 10 \mu\text{m/ns}$ or 2-eV equivalent temperature).

Adding high-Z gas into the NIF Marble capsule showed the ability to control the degree of heterogeneous mix by preserving initial pore size of the Marble foam. However, the geometry and highly heterogeneous structure make it difficult to confirm this. Therefore, the single-void collapse platform (previously filled with foam, now filled with krypton gas) was modified to test how a void collapses and deforms under different high-Z gas pressure conditions. Figure 23 shows the chlorine backlighter images taken with a mixture of 3 atm of krypton gas and 3 atm of hydrogen. Figure 23(a) shows an image taken before the shock reaches the initial gas-filled void, which appears to have substantially compressed even prior to shock arrival. This is expected according to simulations. Figure 23(b) shows a late-time image taken after the shock reaches the void, which is flattened during interaction with the shock. Our target leaking during the shot presented an experimental challenge. In the future, high-pressure target designs will require further refinement.



U2518JR

Figure 23

(a) An image taken before the shock reaches the initial gas-filled void and (b) an image taken after the shock reaches the initial gas-filled void.

This work was performed under the auspices of the U.S. Department of Energy by the Triad National Security, LLC, at Los Alamos National Laboratory. MARBLE is supported by the DOE NNSA Office of Experimental Science (NA-113) SAT and PAT Programs.

1. K. Molvig *et al.*, Phys. Rev. Lett. **116**, 255003 (2016).
2. B. Scheiner *et al.*, Phys. Plasmas **26**, 072707 (2019).
3. A. S. Liao *et al.*, Phys. Plasmas **26**, 032306 (2019).
4. C. Graziani *et al.*, Rev. Sci. Instrum. **88**, 123507 (2017).